A Journal of the Gesellschaft Deutscher Chemiker

Angewandte International Edition GDCh Chemie

www.angewandte.org

## Accepted Article

**Title:** Near-infrared Light-triggered Chlorine Radicals (•Cl) Stress for Cancer Therapy

**Authors:** Ruixue Song, Han Wang, Meng Zhang, Yanyan Liu, Xianfu Meng, Shaojie Zhai, Chao-chao Wang, Teng Gong, Yelin Wu, Xingwu Jiang, and Wenbo Bu

This manuscript has been accepted after peer review and appears as an Accepted Article online prior to editing, proofing, and formal publication of the final Version of Record (VoR). This work is currently citable by using the Digital Object Identifier (DOI) given below. The VoR will be published online in Early View as soon as possible and may be different to this Accepted Article as a result of editing. Readers should obtain the VoR from the journal website shown below when it is published to ensure accuracy of information. The authors are responsible for the content of this Accepted Article.

**To be cited as:** *Angew. Chem. Int. Ed.* 10.1002/anie.202007434

**Link to VoR:** https://doi.org/10.1002/anie.202007434

WILEY-VCH

10.1002/anie.202007434

WILEY-VCH

RESEARCH ARTICLE

# Near-infrared Light-triggered Chlorine Radicals (•Cl) Stress for Cancer Therapy

Ruixue Song,[a] Han Wang,[c] Meng Zhang,[c] Yanyan Liu,*[a, b] Xianfu Meng,[d] Shaojie Zhai,[c] Chao-chao Wang,[d] Teng Gong,[a] Yelin Wu,[d] Xingwu Jiang,[b] and Wenbo Bu*[a, b, c]

[a] R. Song, Prof. Y. Liu, Dr. T. Gong, Prof. W. Bu
Shanghai Key Laboratory of Green Chemistry and Chemical Processes
School of Chemistry and Molecular Engineering, East China Normal University
Shanghai 200062, P. R. China
E-mail: wbbu@chem.ecnu.edu.cn; liuyanyan@chem.ecnu.edu.cn

[b] Prof. Y. Liu, Dr. X. Jiang, Prof. W. Bu
Department of Materials Science
Fudan University
Shanghai 200433, P.R. China
E-mail: wbbu@fudan.edu.cn

[c] Dr. H. Wang, Dr. M. Zhang, S. Zhai, Prof. W. Bu
State Key Laboratory of High Performance Ceramics and Superfine Microstructure
Shanghai Institute of Ceramics, Chinese Academy of Sciences
Shanghai 200050, P. R. China

[d] Dr. X. Meng, Dr. C. Wang, Prof. Y. Wu
Tongji University Cancer Center
Shanghai Tenth People's Hospital, Tongji University School of Medicine
Shanghai 200072, P. R. China

Supporting information for this article is given via a link at the end of the document.

**Abstract:** Free radicals with reactive chemical properties can battle against tumors without causing drug resistance. Reactive oxygen species (ROS) has been widely used for cancer treatment, but regrettably, the common existence of $O_2$ and $H_2O_2$ deficiency in tumor set a severe barrier for sufficient ROS production, leading to unsatisfactory anticancer outcomes. Here, we construct chlorine radical (•Cl) nano-generator with inner upconversion nanoparticle (UCNP) coated by $SiO_2$, and decorated with $Ag^0$/AgCl hetero-dots outside. Upon near-infrared (NIR) light irradiation, the short-wavelength emission UCNP catalyzes $Ag^0$/AgCl for •Cl generation with no dependence on $O_2$/$H_2O_2$. •Cl with strong oxidability and nucleophilicity can attack biomolecules in cancer cells more effectively than ROS. This •Cl stress treatment will no doubt broaden the family of oxidative stress-induced antitumor strategy by using non-oxygen free radicals, which is significant for reference in the development of new anticancer agents.

## Introduction

Cancer cells underdo severe oxidative stress due to multiple genetic mutation and metabolic alteration, making them more vulnerable to further insults of oxidative species than normal cells.[1] Based on this biochemical characteristic, many anticancer drugs are developed with the ability of free radicals production.[2] Free radicals with unpaired electrons are chemically oxidative.[3] They tend to take electrons from surrounding substances (such as lipids, proteins and DNA), and trigger the domino effect passing on the chain reaction of oxidation.[4] As such, free radicals can battle against all types of tumors without causing drug resistance.[5] Certain free radicals-based antitumor strategies include traditional radiotherapy and chemotherapy[6], and some novel therapies like photodynamic therapy (PDT)[7] and chemodynamic therapy (CDT)[8], all of which can stimulate the generation of ROS (including •OH, $O_2$•$^-$, and $^1O_2$) to increase ROS stress in cells. However, there is a huge barrier for sufficient production of ROS to get satisfactory anticancer outcomes, as the common existence of hypoxia and $H_2O_2$ in tumor is deficient for tumor therapy, whereas the yield of ROS relies heavily on $O_2$ and $H_2O_2$ concentrations in tumor.[9] From this point, exploring other available free radicals without dependence on $O_2$ and $H_2O_2$ may be feasible alternatives for efficient tumor therapy. [10]

Chlorine radical (•Cl) with strong oxidation characteristics has been an appealing option for organic pollutant removal in wastewater treatment processes.[11] Its oxidation potential of 2.47 V is second only to hydroxyl radical (•OH, 2.80 V) [12], but its generation is thermo-dynamically easier, meaning a longer lifespan and diffusion distance for efficient oxidative reaction.[13] More importantly, in contrast to •OH, •Cl shows stronger and faster reactivity to certain electron-rich substances by nucleophilic addition,[14] thus can attack cells more effectively due to the abundant presence of nucleophilic atoms and functional groups in biomolecules. Electrophilic reaction of $Cl_2$•$^-$ (2.0 V) as reported,[15] can form chlorine atom adduct to impede DNA replication or transcription, where $Cl_2$•$^-$ is the product of diminished •Cl.[16] •Cl may further cause one-electron oxidation with DNA skeletons to inflict severe cellular damage directly. So •Cl may have enormous potential for highly effective •Cl stress tumor killing. At present, •Cl is commonly produced by either electrocatalysis or photocatalysis of chloride salt solution or halogenated hydrocarbon.[17] Considering that $Cl^-$ is one of the most abundant components in living organisms, it is a natural advantage for sufficient supply of chloride source, but still a challenge for efficient formation of •Cl via catalytic reaction under physiological conditions.

Here, we designed and constructed the •Cl nano-generators for •Cl stress antitumor therapy, with inner upconversion


This article is protected by copyright. All rights reserved.

Accepted Manuscript

10.1002/anie.202007434




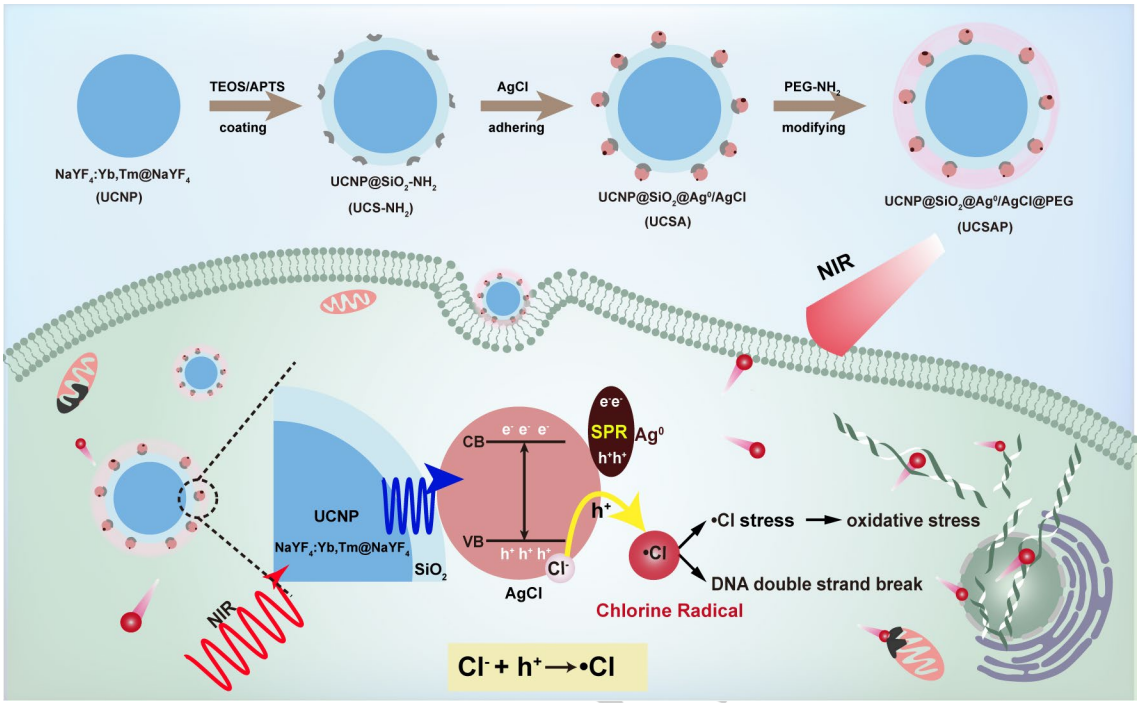


**Scheme 1.** Schematic diagram of UCSAP synthesis and chlorine radical (•Cl) generation upon NIR irradiation for •Cl stress tumor therapy. Upon NIR light irradiation, the short-wavelength emission light of UCNP catalyzes $Ag^0$/AgCl generating electron-hole pairs. The photogenic holes further oxidize $Cl^-$ for •Cl generation, which can induce tumor cells •Cl stress and DNA double-strand break.

nanoparticles (UCNPs) coated by $SiO_2$ and decorated with $Ag^0$/AgCl hetero-dots outside (named as UCSAP). Upon near-infrared (NIR) light irradiation, the short-wavelength emission of UCNP can stimulate the generation of electron-hole pairs in $Ag^0$/AgCl. Additionally, the photogenic holes can further oxidize $Cl^-$ for •Cl generation, as seen in Scheme 1. Importantly, the surface plasmon resonance (SPR) effect of $Ag^0$[18] will largely contribute to the absorption of $Ag^0$/AgCl in the ultraviolet and visible region. Moreover, the heterostructure of $Ag^0$/AgCl favored the transfer of photogenic electrons to each other, so as to effectively separate hole-electron for sufficient generation of •Cl.[11a, 19] Thus, by combining photomodulator of UCNP and photocatalysis of $Ag^0$/AgCl, upon NIR stimulation, the electrophilic •Cl of strong oxidation can be generated with no dependence on $O_2$/$H_2O_2$. *In vitro* and *in vivo* results suggest the effective generation of •Cl to induce •Cl stress in both normoxia and hypoxic tumors. This method may lead to the new trend of free radical-induced tumor therapy, and provide a reference for the development of non-oxygen free radicals for future oxidative stress antitumor therapy.

## Results and Discussion

**Characterization of UCSAP.** The UCNP luminescent core coated with silica (UCNP@dSiO$_2$) was synthesized as the previous method.[20] In brief, a layer of NaYF4 was grown on the surface of the $NaYF_4$:20%Yb,0.5%Tm core by two-step pyrolysis. Both $NaYF_4$:Yb,Tm (Supplementary figure 1a) and $NaYF_4$:Yb,Tm@$NaYF_4$ (Supplementary figure 1b) had excellent crystallinity and uniform morphology in TEM images, and the outer coating of $NaYF_4$ showed a satisfactory luminescence enhancement effect with blue and violet light emission under 980 nm laser irradiation (Supplementary figure 2). After being coated with $SiO_2$, UCNP@dSiO$_2$ also showed uniform morphology in TEM images (Figure 1a), and the further modification of amino groups (-$NH_2$) was determined by FT-IR spectra (Supplementary figure 3).[21] The extremely small-sized $Ag^0$/AgCl hetero-dot was synthesized by the reverse microemulsion method. $Ag^0$/AgCl could adhere to the UCNP@$SiO_2$ exterior via strong interactions between -$NH_2$ and $Ag^0$/AgCl to form UCNP@$SiO_2$@$Ag^0$/AgCl. X-ray powder diffraction (XRD) pattern of the UCSA revealed that the nanoparticles were successfully synthesized with the presence of both the hexagonal phase of $NaYF_4$ (JCPDS PDF#16-0334) and the cubic phase of AgCl (JCPDS PDF#31-1238) (Figure 1d). Transmission electron microscope (TEM) images showed that UCSA had a uniform morphology with the super-small spherical AgCl at a diameter of ~ 4 nm adhering to the outer surface of UCNP@$SiO_2$ (Figure 1 b-c). Finally, UCNP@$SiO_2$@$Ag^0$/AgCl was modified with PEG-$NH_2$ for UCNP@$SiO_2$@$Ag^0$/AgCl@PEG (UCASP) with improved biocompatibility. The dynamic light scattering (DLS) results of UCAS and UCASP NPs proved their excellent stability and dispersion in water, cell culture medium, and serum (Supplementary figure 4), ensuring their further application both *in vitro* and *in vivo*.

UV-Vis spectra indicated that the absorption of $Ag^0$/AgCl was in the range of 250 to 800 nm (Figure 1e). This matches well with



This article is protected by copyright. All rights reserved.

Accepted Manuscript

10.1002/anie.202007434




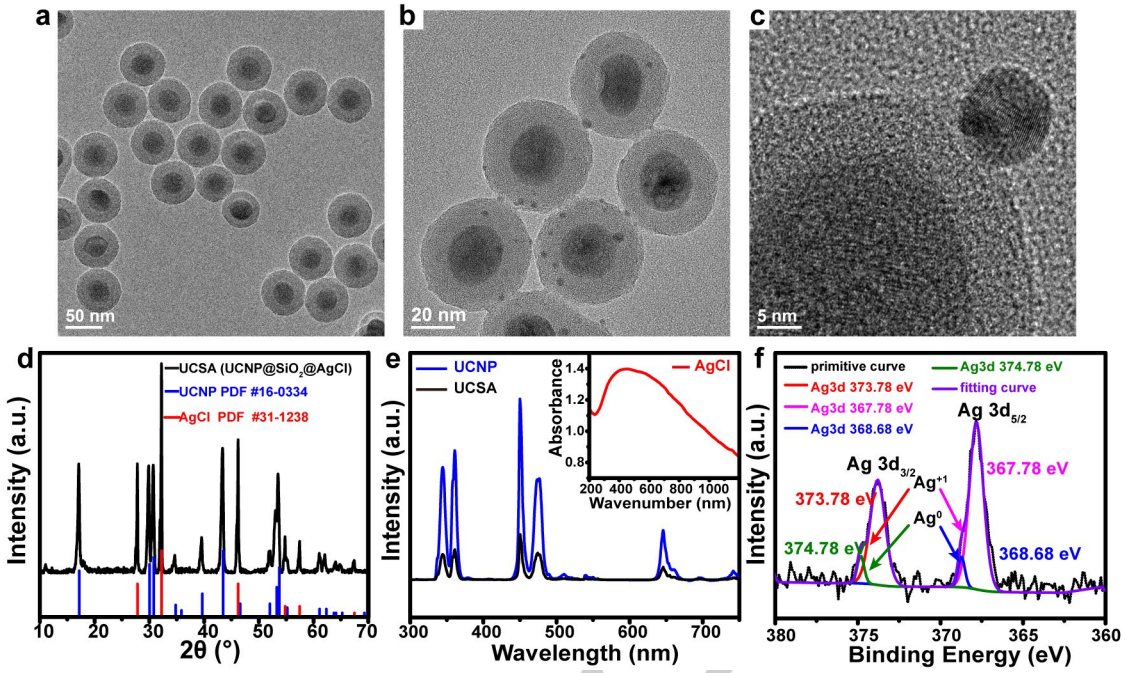


**Figure 1.** Characterization of UCSAP NPs. (a) TEM images of UCNP@$SiO_2$ (UCS) nanoparticles. (b-c) TEM images of UCNP@$SiO_2$@$Ag^0$/AgCl (UCSA) nanoparticles. (d) XRD patterns of as-prepared UCSA nanoparticles. (e) Luminescence emission spectra of UCNP (Y, 174 mg/L) in cyclohexane and UCSA (Y, 174 mg/L; Ag, 20 mg/L) in DI water under 980 nm light excitation (P = 0.36 W/$cm^2$). The insertion graph is the UV-Vis absorption spectrum of $Ag^0$/AgCl (Ag, 20 mg/L). (f) Ag 3d XPS spectra of UCSA.

the fluorescence emission spectra of UCNP upon 980 nm excitation (Figure 1e), assuring the NIR-photocatalytic process of $Ag^0$/AgCl with UCASP. XPS analysis of UCSA showed the co-existence of Ag and Cl on the surface of UCSA (Supplementary figure 5). Ag 3d spectrum showed two banding energies contributed by $3d_{3/2}$ and $3d_{5/2}$, indicating the presence of two chemical environments of Ag. The peaks located at 373.78 eV ($3d_{3/2}$) and 367.78 eV ($3d_{5/2}$) could be assigned to $Ag^+$ in AgCl, and the others located at 374.78 eV and 368.68 eV were ascribed to $Ag^0$,[22] indicating the successful synthesis of $Ag^0$/AgCl hetero-dots. This means that the absorption of $Ag^0$/AgCl in both the ultraviolet and visible region was attributed to the surface plasmon resonance (SPR) effect of $Ag^0$ on the AgCl surface. Furthermore, the $Ag^0$/AgCl promotes the transfer of interface electrons and the effective separation of electron-holes in the photocatalytic process.[23] As a result, the photocatalytic efficiency of $Ag^0$/AgCl has been greatly improved to efficiently produce •Cl. Basing on the Fajans Rule, the surfaces of $Ag^0$/AgCl NPs are terminated by $Cl^-$ as proved by the negative zeta potential (Supplementary figure 6). The calculated adsorption energies of $Cl^-$ and $H_2O$ on the surface of $Ag^0$/AgCl are -2.12 eV and -1.03 eV respectively, further meaning the preferential adsorption of $Ag^0$/AgCl for $Cl^-$, but not $H_2O$, which will facilitate the reaction of holes and $Cl^-$ on $Ag^0$/AgCl, and then the generation of •Cl (Supplementary figure 7).

**Generation of •Cl in aqueous solution.** The photocatalytic performance of UCSA under NIR was first tested by methylene blue (MB) degradation experiments. As shown in Figure 2a, MB faded rapidly in the UCSA aqueous solution with the extension of irradiation time under 980 nm light. The decomposition of MB reached approximately 80% within 45 min. However, UCS without $Ag^0$/AgCl didn't degrade MB under the same light conditions (Supplementary figure 8a), and UCSA also didn't decompose MB without light (Supplementary figure 8b). Extra adding chloride salt (0.9% NaCl) in this photocatalytic degradation system gave a faster degradation rate of MB than that in DI water (Supplementary figure 9), meaning the introduction of $Cl^-$, chlorine source can support the high-efficient generation of •Cl. Then, the N,N-diethyl-p-phenylenediamine (DPD) standard method was used to verify the production of free chlorine during the photo-catalytic process.[12] As shown in Figure 2b, the double-peak absorbance spectrum at 515 nm and 553 nm was DPD intermediates known as a Würster dye formed by colorless DPD and free chlorine. Furthermore, the absorbance peak gradually increased under exposure to UV light, indicating the effective production of free chlorine by UCSA upon light irradiation. Furthermore, the ESR spin trapping technique was performed to confirm the generation of •Cl by $Ag^0$/AgCl. DMPO was employed as the trapping agent of •Cl. As shown in Figure 2c, a seven-line ESR spectrum of DMPOX, which is identified as the oxidized derivative of DMPO *via* •Cl oxidation,[24] appeared in the mixture of DMPO and UCSA when exposed to NIR light, intuitively showing the generation of •Cl by this NIR-photocatalysis of $Ag^0$/AgCl. In addition, the chlorinated products of cinnamyl alcohol were determined by gas chromatography-mass spectrometry (GC-MS) after the photocatalytic reaction of cinnamyl alcohol with UCSA, which further demonstrated the production of •Cl (Figure 2d and Supplementary figure 10). All the above results provided reliable experimental evidence to support the successful generation of •Cl by UCSA nanoplatform under light excitation.

**The formation mechanism of •Cl.** The bandgap of semiconductor AgCl is 3.25 eV.[25] When the exposed light photon



This article is protected by copyright. All rights reserved.

Accepted Manuscript

10.1002/anie.202007434




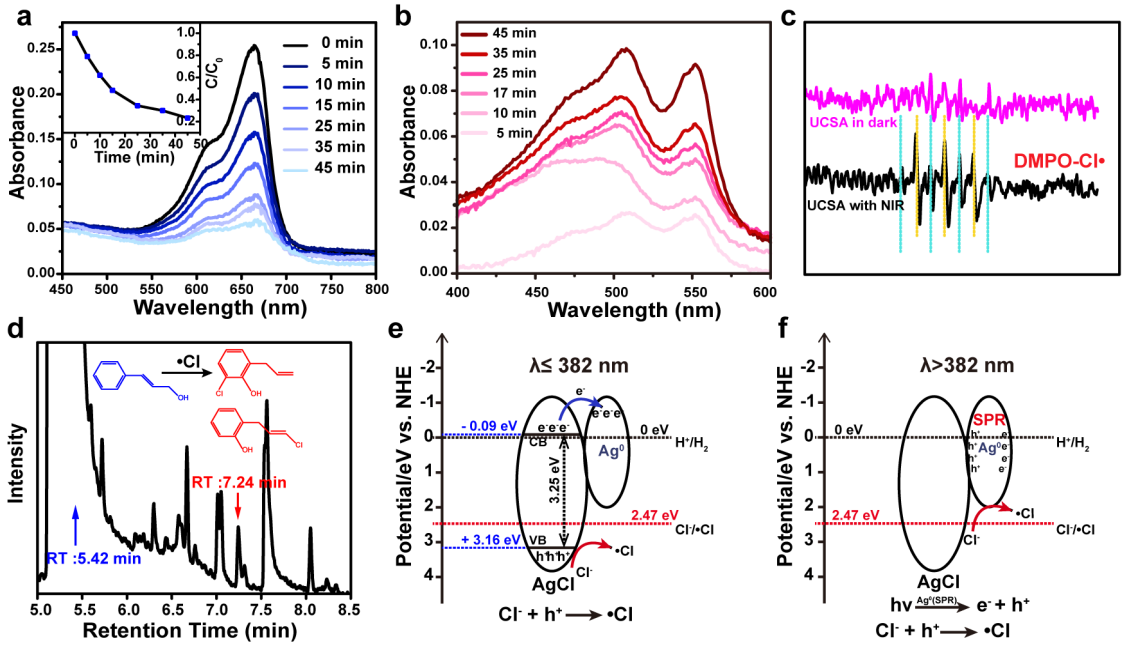


**Figure 2.** The ability of UCSAP to produce •Cl in aqueous solution was verified. (a) The varying UV-vis absorption spectra of MB aqueous solution under NIR irradiation (P = 1.4 W/cm$^2$) in the presence of UCSA. The inserted graph shows the relative concentration of MB during the degradation process over time. C represents the concentration of MB at time t, and $C_0$ represents the initial concentration of MB before photodegradation. (b) The time-dependent UV-vis absorption spectrum of DPD with continuous irradiation. The increasing absorption intensity at 515 nm indicates the oxidized product of DPD by free chlorine species, which is produced by UCSA under light irradiation. (c) ESR spectra of DMPO capturing •Cl generated by UCSA upon NIR irradiation. (d) The gas chromatography of cinnamyl alcohol was obtained after the photocatalytic reaction of cinnamyl alcohol with UCSA. The retention time of 5.42 min was cinnamyl alcohol, and the retention time of 7.24 min was the chlorinated adduct of cinnamyl alcohol. Their corresponding mass spectra are shown in Supplementary figure 10. (e-f) Schematic illustration of $Ag^0$/AgCl poyocatalytic production of •Cl.

energy on $Ag^0$/AgCl is greater than or equal to 3.25 eV, AgCl would be excited to generate electron-hole pairs; otherwise, $Ag^0$ would absorb photons to generate electrons and holes. According to Planck's Formula (Eq. (1)), the boundary between the two processes depends on whether the wavelength of the emitted light of UNCP is greater or less than 382 nm. Since UCNP emits light in the range of 300-800 nm (Supplementary figure 2), both photocatalytic processes of $Ag^0$/AgCl occur (Figures 2e and 2f). Specifically, AgCl will generate the photogenic electron-hole pairs after the absorption of UV light (Eq. (2)). The photogenic electrons transfer to the metal elemental $Ag^0$ promoting the separation of electron-hole pairs, and the hole left will oxidize $Cl^-$ to generate •Cl (Eq. (3))[26].

$$\mathrm{E} = h\nu = \frac{hc}{\lambda} \quad (1)$$

$$AgCl \xrightarrow{h\nu} AgCl + h^+ + e^- \quad (2)$$

$$h^+ + Cl^- \rightarrow \bullet Cl \quad (3)$$

$$\mathrm{h}\nu \xrightarrow{Ag^0(SPR)} e^- + h^+ \quad (4)$$

When $Ag^0$/AgCl is put under visible light (λ>382 nm), the $Ag^0$ absorbs photons and separates them into electrons and holes through the SPR effect (Eq. (4)). The holes would oxidize $Cl^-$ to •Cl (Eq. (3)).

**•Cl therapy *in vitro*.** Since UCSA nanoparticles had superior •Cl productivity and excellent organic dye degradation performance under NIR irradiation, its cell-killing effect was subsequently verified *in vitro*. There was no obvious ion release from UCSAP (Supplementary figure 11), and no •Cl production in serum with UCSAP without light irradiation (Supplementary figure 12), meaning the insignificant dark toxicity of UCSAP. It is worth mentioned that the nanosystem could be significantly endocytosed by 4T1 cells, which was observed using FITC labeled UASAP under confocal laser scanning microscopic (CLSM) (Supplementary figure 13). The biosafety of UCSAP *in vitro* was evaluated on human embryonic kidney 293 cells (HEK293) and mice Kupffer cells. The survival rates of both Kupffer cells and HEK293 cells were greater than 80% after 24 h of co-culturation with UCSAP in dark (Supplementary figure 14). In contrast, UCSAP NPs showed an obvious killing effect upon 980 nm laser irradiation (P = 1.4 W/cm$^2$, t = 3 min) to both normoxic and hypoxic 4T1 cells (Figure 3a), with the IC50 of NPs decreasing from 337 μg/mL in dark to 70 μg/mL (normoxia, $pO_2$: 21%) and from 284 μg/mL in dark to 59 μg/mL (hypoxia, $pO_2$: 2%) (Supplementary figure 15), indicating the excellent NIR-induced cytotoxicity of UCSAP with no dependence on oxygen. Similar therapeutic effects were acquired on human lung cancer (A549) cells and human cervix cancer (HeLa) cells, meaning the universal cytotoxicity of UCSAP/NIR (Supplementary figure 16).

To characterize the action mechanism of UCSAP, the cytotoxicity of UCNP@$SiO_2$ (UCS) without $Ag^0$/AgCl dots was tested. The cell survival rates of normoxic/hypoxic 4T1 cells with/without NIR irradiation all kept above 80% even the concentration of UCNP@$SiO_2$ high to 400 μg/mL, suggesting the excellent biosafety of UCNP@$SiO_2$ (Supplementary figure 17). Apoptosis of 4T1 cells was further assessed by flow cytometry analysis. Groups treated with PBS, PBS/NIR, UCS, or USC/NIR showed similar apoptosis at a rather low ratio, meaning their little



This article is protected by copyright. All rights reserved.

Accepted Manuscript

10.1002/anie.202007434




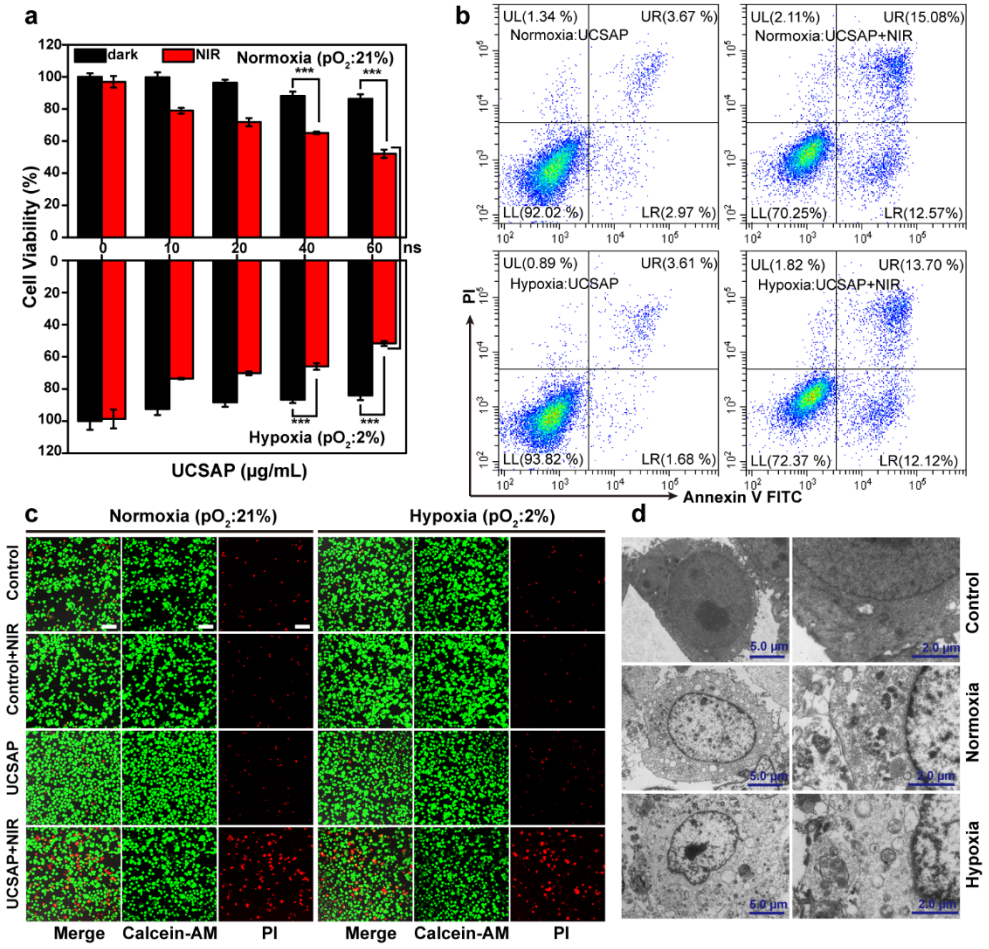


**Figure 3.** UCSAP NPs could efficiently cause tumor cell death under NIR-trigger. (a) Cytotoxicity of UCSAP to both normoxic and hypoxic cells with or without NIR irradiation; n = 6, mean ± SD; statistical analysis was assessed by two-way ANOVA test (***p<0.001). (b) Flow cytometry analysis staining with Annexin V-FITC/PI in apoptosis of 4T1 cells treated with UCSAP (32 μg/mL) and UCSAP/NIR (32 μg/mL) under both normoxia ($pO_2$: 21%) and hypoxia ($pO_2$: 2%) conditions. Flow cytometry analysis of PBS, PBS/NIR, UCS, and UCS/NIR was in Supplementary figure 18. (c) Confocal microscopic images of 4T1 cells stained with calcein-AM and PI after UCSAP and NIR irradiation treatment. The calcein-AM dye (in green) was used for living cells staining and the PI (in red) for dead cell staining. Scale bar, 100 μm. (d) Bio-TEM images of 4T1 cells before and after UCASP phototherapy, showing the ultrastructure changes of the cells. Scale bar, 5.0 μm (left), 2.0 μm (right).

effect on cells (Supplementary figure 18). However, increased levels of cell death were detected in normoxic/hypoxic cells with UCSAP after NIR irradiation compared to the other treatments (Figure 3b and Supplementary figure 18). In fact, during UCSAP photocatalytic process, $Ag^0$ can generate via one-electron reductive reaction of AgCl, leading to an increased content ratio of $Ag^0/Ag^{+1}$ in $Ag^0$/AgCl samples (Supplementary figure 19). In order to find out whether the increase of $Ag^0$ content in UCSAP would have toxic effects on cells, UCNP@$SiO_2$@$Ag^0$ (UCSAP/$Ag^0$) NPs made by exposing UCSAP to UV lamp for up to 24 h were then evaluated, showing negligible toxicity to 4T1 cells in both normoxia and hypoxia when compared with UCSAP alone at the same conditions (Supplementary figure 20). Therefore, these *in vitro* results clearly demonstrated that the excellent action mechanism of UCSAP NPs was benefited from $Ag^0$/AgCl for photo-triggered •Cl generation as cell killing weapon for tumor therapy. The remarkable cell-killing effects of •Cl could be further verified on 4T1 cells through a live/dead cell assay using calcein-AM/PI dyes under CLSM. While UCSAP was safe for the cells in dark conditions, UCSAP with NIR irradiation had the largest cell killing rate (Figure 3c). In addition, the cell morphology after •Cl therapy was significantly different from that of the untreated cells under bio-electron microscopy. After treatment, the cells showed a morphology typical of apoptotic cells, accompanied by chromatin condensation and fragmentation, endoplasmic reticulum loosening and cavitation, mitochondrial swelling, and apoptosis bodies appeared (Figure 3d).

Since there is no commercial chlorine radical probe at present, DCFH-DA,[27] known as ROS fluorescent probe was used to stain 4T1 cells to detect the change of intracellular oxidative stress, which can indirectly prove the generation of strongly oxidative •Cl. This is because the sharp increase of oxidative substances in cells would disrupt redox homeostasis and further stimulate intracellular oxidative stress.[28] Meanwhile, the strong oxidizing •Cl species would seize electrons from the surrounding water, proteins, lipids and other substances to form new free radicals, starting the chain transfer of free radicals' domino effect for enhanced intracellular oxidative stress. As shown in Figure 4a



This article is protected by copyright. All rights reserved.

Accepted Manuscript

10.1002/anie.202007434




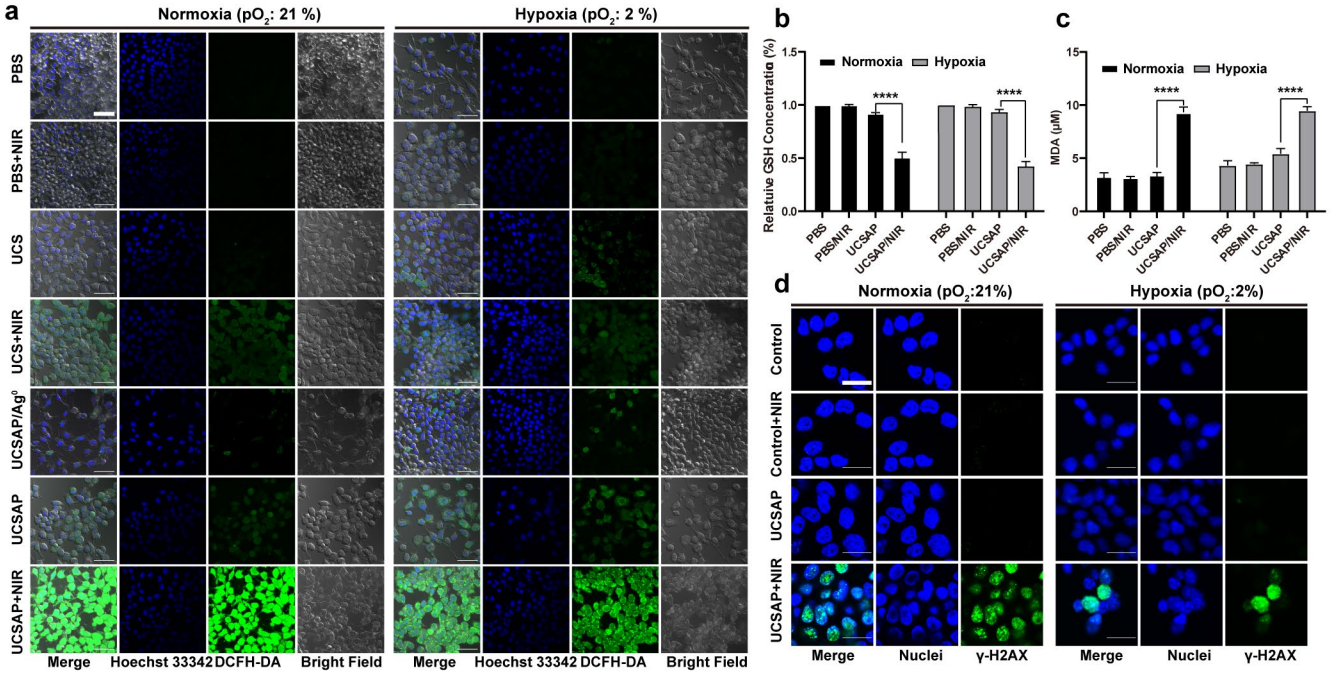


**Figure 4.** The oxidative stress and DNA double-strand breakage in tumor cells. (a) Detection of oxidative stress with DCFH-DA fluorescent probe in both normoxic and hypoxic cells. scale bar, 50 μm. (b) Relative GSH concentration of both normoxic and hypoxic cells treated with UCSAP and NIR irradiation under both normoxic and hypoxic conditions; n = 3, mean ± SD; statistical analysis was assessed by two-way ANOVA test (****p<0.0001). (c) The concentration of MDA in 4T1 cells treated with UCSAP and NIR irradiation under both normoxic and hypoxic conditions; n = 3, mean ± SD; statistical analysis was assessed by two-way ANOVA test (****p<0.0001). (d) Detection of DNA damage with double-strand break in both normoxic and hypoxic 4T1 cells under confocal microscopy with γ-H2AX as immunofluorescence staining. The γ-H2AX was shown in green. The nuclei were stained with Hoechst 33342, shown in blue. Scale bar, 50 μm.

and Supplementary figure 21, the high-fluorescence of DCF as a typical marker of the proliferation of oxidative species was detected in both normoxic and hypoxic cells after treated with NIR irradiation in the presence of UCSAP. In addition, cells were further stained with mitochondrial membrane potential probe, Mitotracker Red CMXRos. As shown in Supplementary figure 22, in comparison to the PBS treatment group, there was a slightly increase of ROS signals in both UCSAP/$Ag^0$ and UCSAP group, without remarkable changes of membrane potential, meaning the insignificant oxidative stress and mitochondrial damage caused by UCSAP/$Ag^0$ or UCSAP. While, in UCSAP/NIR group, the green fluorescence signal dramatically increased with significant damage of the mitochondrial membrane. The underlying mechanism is that when cells treated with UCSAP+NIR, a large amount of strongly oxidizing chlorine radicals could produce to trigger the oxidative stress of cells. The oxidative stress caused by the imbalance of redox is not only manifested as the explosion of oxidation species and the damage of mitochondrial membrane, but also as the decrease of intracellular antioxidants such as glutathione (GSH).[29] After NIR light irradiation, the GSH level decreased significantly in both normoxic and hypoxic cells (Figure 4b), indicating that the generation of strongly oxidative •Cl. In addition, lipid peroxidation with increased malondialdehyde (MDA) concentration in cells was detected in normoxic/hypoxic 4T1 cells treated with UCSAP/NIR, but not in other groups (Figure 4c), indicating that •Cl could cause intracellular lipid peroxidation. However, the reported lipid peroxidation reaction mediated by free radicals does not contain chlorine radicals,[30] whether the intracellular lipid peroxidation of UCSAP/NIR is caused by direct oxidation of phospholipid molecules by •Cl or by •Cl induced biological effect - oxidative stress was still not sure.

Chlorine radicals with high reactivity are prone to electrophilic addition reactions with intracellular biological active substances for instance DNA skeletons, and inhibit DNA replication or transcription through single-electron oxidation of DNA skeletons. In order to verify DNA damage in cells caused by single-electron oxidation of •Cl, the immunofluorescence staining of γ-H2AX analysis was performed, since γ-H2AX is the biomarker of DNA double-strand break[31]. As shown in Figure 4d, while there are almost no green fluorescent spots observed in control group, the additional treatment of UCSAP+NIR revealed obvious green fluorescent spots in both normoxic and hypoxic cells, signifying the UCSAP nano-system in both normoxic and hypoxic tumor cells under NIR excitation could cause intracellular DNA double-strand breakage.

**•Cl therapy *in vivo*.** Encouraged by the great cell-killing effect of •Cl *in vitro*, *in vivo* therapy was carried out on the 4T1 subcutaneous tumor model. After intravenous injection of 50 mg/kg UCSAP into KM mice, the mice's weight was normally increasing within 30 days (Supplementary figure 23). The distribution of UCSAP after 30 days *in vivo* was measured by detecting the amounts of silver elements in their main organs using ICP-OES. The long-term accumulation of Ag in mice was mainly in the liver and spleen, speculating that the liver and spleen are the main metabolic organs of UCSAP NPs (Supplementary figure 24). The corresponding organ histomorphology analysis and blood biochemistry indices showed no abnormalities compared with the control group (Supplementary figure 25-26),



This article is protected by copyright. All rights reserved.

Accepted Manuscript

10.1002/anie.202007434




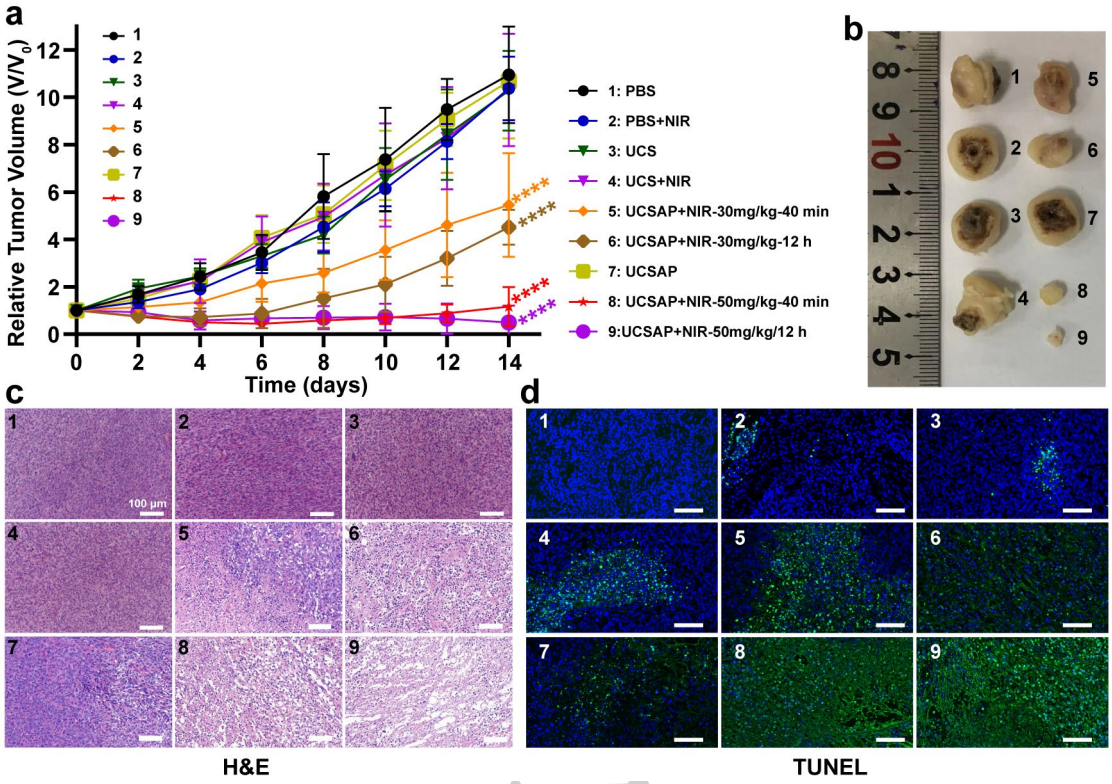


**Figure 5.** ·Cl stress therapy triggered by NIR light could effectively inhibit tumor growth *in vivo*. (a) The changes of relative tumor volume within 14 days after treatment; n = 5, Mean ± SD; statistical analysis was assessed by two-way ANOVA test. (****p<0.0001 versus PBS group). (b) Digital photos of the tumor after treatment for 14 days. (c) H&E and (d) TUNEL staining of the tumor sections two days after treatment. Scale bar, 100 μm.

suggesting the excellent biosafety and biocompatibility of UCSAP, without main toxicological issue caused by the accumulated Ag at such dosage in tissues *in vivo*. To determine the best drug-light interval for *in vivo* treatment, their accumulation at the tumor site was then evaluated by intravenous injection of UCSAP NPs into 4T1 tumor-bearing mice. The tumors were harvested 10 min, 20 min, 40 min, 1 h, 2 h, 3 h, 5 h, 7 h, 12 h and 24 h post-injection to measure Ag concentration in the tumor. As shown in Supplementary figure 27, the enrichment of UCSAP NPs in the tumor was rapid, reaching peak value at 40 min, and then began to decrease slowly to a secondary peak around 7-12 h.

To evaluate their antitumor efficiency, UCSAP NPs with three concentrations (30, 50, and 80 mg/kg) were intravenously injected into 4T1 tumor-bearing mice respectively. Tumors were irradiated with 980 nm (P = 1.4 W/cm$^2$, t = 6 min) after NPs post-injection 40 min or 12 h. Two days later, the corresponding tumors were dissected for TUNEL immunofluorescence staining, showing an increased percentage of the apoptotic area as the increase of UCSAP dose and NPs-light interval (Supplementary figure 28). Although the near-infrared thermal imaging results showed a slight increase in the surface temperature of the tumor area during the treatment of 980 nm light irradiation (Supplementary figure 29-30), the TUNEL staining results of PBS/NIR showed that a slight temperature increase during the light treatment was biosafety. As shown in Figure 5, tumor growth in the group treated with UCSAP NPs at 50 mg/kg plus 980 nm light irradiation at NPs-light 40 min interval (Figure 5, group 8) was significantly suppressed, with a tumor growth inhibition rate (TGI) of ~ 90% after 2-week treatment. The tumor growth was inhibited in 50 mg/kg of UCSAP/NIR groups with 12 h NPs-light interval (Figure 5, group 9), showing similar TGI with 40 min interval (group 8 versus group 9, p > 0.5). By contrast, the TGI becomes lower when decreasing the injection dose of UCSAP NPs to 30 mg/kg, indicating the dose-dependent antitumor efficiency of UCSAP NPs *in vivo*. The H&E and TUNEL staining of tumor tissue sections also revealed that UCSAP had a satisfactory therapeutic effect under NIR light, as tumor cells in groups 8 and 9 showed significant apoptosis (Figure 5 c-d). At 40 min post-injection of 50 mg/kg UCSAP, the enrichment of the UCSAP in the tumor was the maximum, but at that moment NPs may be mainly concentrated in tumor blood vessels. Thus, the better therapeutic effect in group 8 may be due to the fact that the NIR-triggered •Cl destroyed the blood vessels of tumor. Supplementary figure 31 verified our conjecture that both group 8 and group 9 effectively destroyed tumor blood vessels during treatment. In fact, destruction of the tumor vascular system is indeed an effective therapeutic strategy for PDT, because the damaged tumor blood vessels would not only accelerate the accumulation of NPs in the tumor, but also cut off the nutrient supply of the tumor to restrict tumor further growth. In addition, we speculate that the higher concentration of chloride ions in the blood vessels may provide favorable conditions for the production of chlorine radicals under photocatalysis of UCSAP. However, for NPs after 12 h post-injection, they may have entered into tumor intercellular space or intracellular cytoplasm, and the NIR-triggered •Cl could be fully used for improved therapeutic efficacy. Digital photographs of tumor-bearing mice clearly show



This article is protected by copyright. All rights reserved.

Accepted Manuscript

that the UCSAP with NIR irradiation had an excellent tumor inhibitory effect (Supplementary figure 32). The above *in vivo* therapy results revealed that UCSAP with NIR-induced •Cl therapy is an effective anticancer treatment strategy.

## Conclusion

In conclusion, the $Ag^0$/AgCl-decorated UCNP@$SiO_2$ nano-structure was acquired to promote •Cl production in a NIR-photocatalytic process. With strong oxidability and nucleophilicity characteristics, this free radical could induce effective •Cl stress in both normoxic and hypoxic tumor cells. Moreover, its strong and fast reactivity to certain electron-rich substances in cells makes it more attackable to biomolecules, leading to severe cellular damage and final death. Notably, this treatment strategy does not rely on $O_2$/$H_2O_2$, thereby surmounting the obstacle of hypoxia insensitivity in clinical therapy. •Cl can not only trigger the domino effect that passing on the oxidation in a chain reaction and causing intracellular oxidative stress, but also destroy the DNA skeleton leading to the DNA double-strand break. This •Cl stress strategy brings fresh insights and spurs fresh interest to the use of free radicals for tumor treatment, and can provide new ideas for the development of general and efficient antitumor agents with no drug resistance.

## Acknowledgements

The authors would greatly acknowledge the financial support by the National Funds for Distinguished Young Scientists (Grant No. 51725202), the Key Project of Shanghai Science and Technology Commission (Grant No. 19JC1412000), the National Natural Science Foundation of China (Grant No. 51872094), the National Science Foundation for the Young Scientists of China (Grant No. 51702211, 21805090), the National Key R&D Program of China (2018YFA0107900), the Collaborative Innovation Center of Technology and Equipment for Biological Diagnosis and Therapy in Universities of Shandong.

**Keywords:** $Ag^0$/AgCl hetero-dots • chlorine radicals (•Cl) • hypoxia • oxidative stress • UCNP

[1] H. Pelicano, D. Carney, P. Huang, *Drug resistance updates* **2004**, *7*, 97-110.

[2] J. Noh, B. Kwon, E. Han, M. Park, W. Yang, W. Cho, W. Yoo, G. Khang, D. Lee, *Nat. Commun.* **2015**, *6*, 6907.

[3] N. J. Larkins, *Journal of Equine Veterinary Science* **1999**, *19*, 84-85.

[4] a) W. Droge, *Physiological reviews* **2002**, *82*, 47-95; b) G. Perry, A. K. Raina, A. Nunomura, T. Wataya, L. M. Sayre, M. A. Smith, *Free radical biology & medicine* **2000**, *28*, 831-834.

[5] a) D. Trachootham, J. Alexandre, P. Huang, *Nature reviews Drug discovery* **2009**, *8*, 579; b) Q. Cui, J.-Q. Wang, Y. G. Assaraf, L. Ren, P. Gupta, L. Wei, C. R. Ashby Jr, D.-H. Yang, Z.-S. Chen, *Drug Resistance Updates* **2018**; c) L. Wang, Q. Sun, X. Wang, T. Wen, J.-J. Yin, P. Wang, R. Bai, X.-Q. Zhang, L.-H. Zhang, A.-H. Lu, *J. Am. Chem. Soc.* **2015**, *137*, 1947-1955.

[6] C. Gorrini, I. S. Harris, T. W. Mak, *Nature reviews Drug discovery* **2013**, *12*, 931-947.

[7] J. Ge, M. Lan, B. Zhou, W. Liu, L. Guo, H. Wang, Q. Jia, G. Niu, X. Huang, H. Zhou, *Nat. Commun.* **2014**, *5*, 4596.

[8] Z. Tang, Y. Liu, M. He, W. Bu, *Angewandte Chemie International Edition* **2019**, *58*, 946-956.

[9] a) P. C. A. Swamy, G. Sivaraman, R. N. Priyanka, S. O. Raja, K. Ponnuvel, J. Shanmugpriya, A. Gulyani, *Coordination Chemistry Reviews* **2020**, *411*, 213233; b) X. Song, J. Xu, C. Liang, Y. Chao, Q. Jin, C. Wang, M. Chen, Z. Liu, *Nano Lett.* **2018**, *18*, 6360-6368.

[10] X. Q. Wang, F. Gao, X. Z. Zhang, *Angewandte Chemie International Edition* **2017**, *56*, 9029-9033.

[11] a) P. Wang, B. Huang, X. Qin, X. Zhang, Y. Dai, J. Wei, M. H. Whangbo, *Angewandte Chemie International Edition* **2008**, *47*, 7931-7933; b) K. Guo, Z. Wu, C. Shang, B. Yao, S. Hou, X. Yang, W. Song, J. Fang, *Environmental science & technology* **2017**, *51*, 10431-10439.

[12] Y. Ji, J. Bai, J. Li, T. Luo, L. Qiao, Q. Zeng, B. Zhou, *Water research* **2017**, *125*, 512-519.

[13] a) R. Roots, S. Okada, *Radiation research* **1975**, *64*, 306-320; b) C. Lennicke, J. Rahn, R. Lichtenfels, L. A. Wessjohann, B. Seliger, *Cell Communication and Signaling* **2015**, *13*, 39.

[14] a) Y. Xiang, J. Fang, C. Shang, *Water research* **2016**, *90*, 301-308; b) J. Fang, Y. Fu, C. Shang, *Environmental science & technology* **2014**, *48*, 1859-1868; c) Y. Y. Xiang, J. Y. Fang, C. Shang, *Water Research* **2016**, *90*, 301-308.

[15] W.-L. Wang, Q.-Y. Wu, N. Huang, T. Wang, H.-Y. Hu, *Water Research* **2016**, *98*, 190-198.

[16] A. Adhikary, A. Kumar, B. J. Palmer, A. D. Todd, M. D. Sevilla, *J. Am. Chem. Soc.* **2013**, *135*, 12827-12838.

[17] a) C. Tan, B. Xiang, Y. Li, J. Fang, M. Huang, *Chemical Engineering Journal* **2011**, *166*, 15-21; b) H. Park, C. D. Vecitis, M. R. Hoffmann, *The Journal of Physical Chemistry A* **2008**, *112*, 7616-7626.

[18] K. Awazu, M. Fujimaki, C. Rockstuhl, J. Tominaga, H. Murakami, Y. Ohki, N. Yoshida, T. Watanabe, *J. Am. Chem. Soc.* **2008**, *130*, 1676-1680.

[19] J. Ke, C. Niu, J. Zhang, G. Zeng, *Journal of Molecular Catalysis A: Chemical* **2014**, *395*, 276-282.

[20] R. Song, M. Zhang, Y. Liu, Z. Cui, H. Zhang, Z. Tang, X. Chen, H. Wu, Z. Yao, M. He, W. Bu, *Biomaterials* **2018**, *175*, 123-133.

[21] W. Y. D. Yong, Z. Zhang, G. Cristobal, W. S. Chin, *Colloids and Surfaces A: Physicochemical and Engineering Aspects* **2014**, *460*, 151-157.

[22] L. Han, P. Wang, C. Zhu, Y. Zhai, S. Dong, *Nanoscale* **2011**, *3*, 2931-2935.

[23] S. Zhang, J. Li, X. Wang, Y. Huang, M. Zeng, J. Xu, *ACS applied materials & interfaces* **2014**, *6*, 22116-22125.

[24] T. Li, Y. Jiang, X. An, H. Liu, C. Hu, J. Qu, *Water research* **2016**, *102*, 421-427.

[25] J. Tejeda, N. Shevchik, W. Braun, A. Goldmann, M. Cardona, *Phys Rev B* **1975**, *12*, 1557.

[26] L. Qi, J. Yu, G. Liu, P. K. Wong, *Catal Today* **2014**, *224*, 193-199.

[27] M. Afri, A. A. Frimer, Y. Cohen, *Chem Phys Lipids* **2004**, *131*, 123-133.

[28] J. Kim, J. Kim, J.-S. Bae, *Experimental & Molecular Medicine* **2016**, *48*, e269-e269.

[29] S. Shrivastava, M. K. Jeengar, V. S. Reddy, G. B. Reddy, V. G. M. Naidu, *Experimental and Molecular Pathology* **2015**, *98*, 313-327.

[30] E. Niki, *Free Radical Biology and Medicine* **2009**, *47*, 469-484.

[31] A. Kinner, W. Wu, C. Staudt, G. Iliakis, *Nucleic Acids Res* **2008**, *36*, 5678-5694.



This article is protected by copyright. All rights reserved.

Accepted Manuscript

10.1002/anie.202007434

WILEY-VCH

RESEARCH ARTICLE

## Entry for the Table of Contents

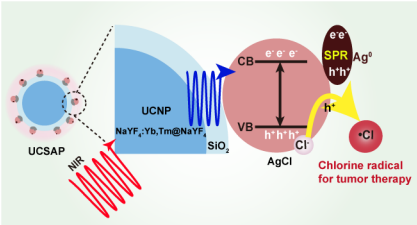


Chlorine radical (•Cl) nano-generator is constructed with the inner upconversion nanoparticle (UCNP) coated by $SiO_2$ shell with $Ag^0$/AgCl hetero-dots decorated outside. Upon NIR light irradiation, the upconversion emission light of UCNP activates $Ag^0$/AgCl to catalyze $Cl^-$, forming •Cl with strong oxidability and nucleophilicity, without dependence on $O_2$ and $H_2O_2$ for efficient tumor therapy.

WILEY-VCH

Accepted Manuscript


This article is protected by copyright. All rights reserved.